

Image Restoration Based on Edgemap and Wiener Filter for Preserving Fine Details and Edges

S. Suhaila, and T. Shimamura

Abstract—This paper presents a method for removing noise while preserving the image fine details and edges in blind condition, based on the Wiener filter and a constructed edgemap. The noisy image is denoised with different weights of Wiener filtering to generate two restored images; one with highly reduced noise, and the other with preserved fine details and edges. The edgemap image is constructed directly from the noisy image by using a new edge detection method. The Wiener filtered images and the edgemap are utilized to generate the final restored image. Simulations with natural images contaminated by noise demonstrate that the proposed method works effectively over a different range of noise levels. A performance comparison with other Wiener filter-based denoising methods and the state-of-the-art denoising methods is also made.

Keywords— Edgemap, Image denoising, Power spectrum estimation, Wiener filter.

I. INTRODUCTION

ALTHOUGH image denoising has been researched quite extensively, developing a denoising method that could remove noise effectively without eliminating the image fine details and edges is still a challenging task. Until recent years, many denoising methods have been proposed [1]-[5]. Some recent non-linear methods suggest employing different denoising approaches for the smooth and non-smooth regions. This type of technique is proposed in the adaptive Total Variation (ATV) [3] and the non-local means (NLM) [4] methods. Conversely, linear methods such as the Wiener filter [6] balance the tradeoff between inverse filtering and noise smoothing. The Wiener filter eliminates the additive noise while inverting blurring.

The Wiener filter is the best known technique for the linear image denoising [7]. It has been implemented for image denoising in several transform domains, for example the spatial domain [8],[9], and the frequency domain [10],[11]. Recently, the wavelet-based denoising methods have dominated the latest research trend in image processing. The Wiener filter

This study was supported and sponsored by Saitama University, Malaysia Ministry of Higher Education (MOHE) and Tun Hussein Onn Malaysia University (UTHM).

S. Suhaila is with the Graduate School of Science and Engineering, Saitama University, Saitama, Japan, 338-8570 (phone: 81-48-858-3496; fax: 81-48-858-3716; e-mail: suhaila_bs@sie.ics.saitama-u.ac.jp).

T. Shimamura is with the Graduate School of Science and Engineering, Saitama University, Saitama, Japan, 338-8570 (e-mail: shima@sie.ics.saitama-u.ac.jp).

implemented in the wavelet domain by using the first generation wavelet has been introduced in many papers, for example in [12],[13]. The second generation wavelet: lifting-based wavelet has been introduced by Sweldens [14] to help reducing computation, which also achieves lossy to lossless performance with a finite precision [15]. The lifting-based wavelet domain Wiener filter (LBWDWF) [16] shows substantial improvement in the restoration performance, and provides much faster computation in comparison to the classical wavelet domain Wiener filter [18]. In practical cases, the information of the original image and the noise level is unknown (blind condition). Thus, to utilize the Wiener filter, noise estimation plays an important role to accomplish accurate denoising. The Wiener filter applied in the spatial domain, the adaptive Wiener filter (AWF), as suggested by Lee [8], first estimates the local variances from the neighborhood around each pixel. The average of these estimates is subsequently used to estimate the noise variance. Methods to estimate the noise variance for the spatial domain Wiener filter are also proposed in [17],[18]. Alternatively, several power spectrum estimation methods have been proposed for estimating noise in the frequency domain [19]-[22]. However, there are a few applied for direct implementation in the frequency domain Wiener filter [10], [11].

The ATV utilizes the idea of the Total Variation (TV) [23]. The TV searches for the minimal energy functional to reduce the total variation of the image via a global power constraint. On the other hand, the ATV reduces the total variation of the image adaptively. It employs strong denoising in the smooth regions and weak denoising in the non-smooth regions. The NLM measures the similarity of the grey level between two pixels. It also compares the geometrical configuration adapted to the local and non-local geometry of the whole image. The methods such as the LBWDWF, ATV and NLM are reported to have superior performance in noise removal and preservation of strong edges. They, however, share a common drawback: that is, the fine details and edges of the original image are not well preserved in the restored image, especially in higher noise environments.

To overcome this problem, a frequency domain Wiener filter-based denoising has been proposed in [20]. We refer this method to as the frequency domain Wiener filter (FDWF). The FDWF introduces a noise and image power spectra estimation method for the implementation of the Wiener filter in blind condition. The FDWF provides the preservation of the fine details and edges, but a certain level of noise remains in the restored

image.

In this paper, we propose a denoising technique to preserve the image fine details and edges while effectively reducing the noise level. The proposed method is based on the FDWF. The image restored by using the FDWF with a low threshold value is utilized in the non-smooth regions in the final restored image. Conversely, the image restored by using the FDWF with a high threshold value is employed in the smooth regions in the final restored image. A new edge detection method is derived and incorporated in the proposed method to distinguish between the smooth and non-smooth regions effectively in the presence of noise. The edge detection is performed in four directions and the results are combined to construct an edgemap. The final restored image is constructed by assigning the smooth and non-smooth regions based on the edgemap. Simulation results verify a significant reduction of the noise level in the smooth regions relative to that of the FDWF.

The paper is organized as follows. We begin with the introduction of the FDWF in Section II, and then describe the proposed denoising method in Section III. In Section IV, we discuss the simulation results and the performance comparison of our method. In Section V, we draw concluding remarks.

II. FDWF

Our procedure for image denoising utilizes the FDWF proposed in [24]. We assume that the image is corrupted by independent additive zero-mean Gaussian white noise. A noisy image, $h(u,v)$, corrupted by the noise, $n(u,v)$, can be expressed as

$$h(u,v) = p(u,v) + n(u,v) \quad (1)$$

where $p(u,v)$ represents the original image. The FDWF employs a threshold process to estimate the image and noise power spectra. The assumption is that in general, the noise power spectrum usually occupies high frequencies, and conversely the image power spectrum is commonly concentrated at low frequencies.

First, we transform the noisy image $h(u,v)$ to the frequency domain, $\hat{h}(s,t)$, by using the fast Fourier transform (FFT). The power spectrum of $\hat{h}(s,t)$, $H(s,t)$, is obtained by

$$H(s,t) = |\hat{h}(s,t)|^2 \quad (2)$$

and the logarithmic power spectrum of $H(s,t)$, $G(s,t)$, is given by

$$G(s,t) = \log(H(s,t)). \quad (3)$$

We perform the estimation for the power spectra of the image and noise block-by-block. $H(s,t)$ and $G(s,t)$ are assumed as blocks. They are divided into $k \times k$ non-overlapping sub-blocks. $H_{(i,j)}(s,t)$ and $G_{(i,j)}(s,t)$ correspond to the (i,j) th sub-block of $H(s,t)$ and $G(s,t)$, respectively.

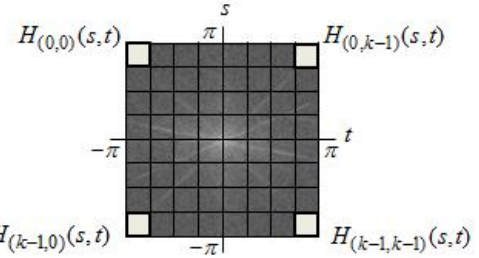


Fig.1 Average of four corners (highest frequencies)

Next, we compute the average of the logarithmic power spectrum in each $G_{(i,j)}(s,t)$ sub-block, which is denoted as $\bar{G}_{(i,j)}(s,t)$, respectively. We find from all the image's sub-blocks the $\bar{G}_{(i,j)}(s,t)$ that represent the minimum and median values of the entire $\bar{G}_{(i,j)}(s,t)$ as \bar{G}_{min} and \bar{G}_{med} , respectively. The minimum value \bar{G}_{min} and the median value \bar{G}_{med} are substituted in the following global threshold value as

$$\alpha = \bar{G}_{med} \cdot \frac{\lambda}{100} + \bar{G}_{min} \quad (4)$$

where λ denotes a division ratio of \bar{G}_{med} , and α corresponds to the threshold value used for the power spectrum estimation. The frequencies that are higher than α correspond to the low frequency regions, while those smaller than α correspond to the high frequency regions. The λ is essential to adjust the specific fraction of the median value \bar{G}_{med} . When λ is set to be low, the threshold value α will be low, thus more frequencies will be included into low frequency regions. Conversely, if λ is set to be high, the threshold value α will be high, thus more frequencies will be included into high frequency regions. Therefore, λ plays an important role in the threshold value decision.

The utilization of \bar{G}_{med} in (4) is attributed to the fact that the median represents where most of the power spectrum concentrated. If the division of the high and low frequencies considers the main power concentration via median, the threshold value will be robust to the variation of the power spectrum characteristics in different images.

The noise power spectrum is estimated from both high and low frequency regions, since we consider that the noise occupies both regions. In high frequency region, the image power spectrum, $P_{(i,j)}(s,t)$, and the noise power spectrum, $N_{(i,j)}(s,t)$, in the corresponding sub-block are approximated by

$$\begin{aligned} & \text{if } \bar{G}_{(i,j)}(s,t) \leq \alpha, \\ & \text{then } P_{(i,j)}(s,t) = 0, N_{(i,j)}(s,t) = H_{(i,j)}(s,t). \end{aligned} \quad (5)$$

In low frequency region, $P_{(i,j)}(s,t)$ and $N_{(i,j)}(s,t)$ are estimated as

$$\begin{aligned} & \text{if } \bar{G}_{(i,j)}(s,t) > \alpha, \\ & \text{then } P_{(i,j)}(s,t) = H_{(i,j)}(s,t), \\ & N_{(i,j)}(s,t) = \text{average} [H_{(0,0)}(s,t), H_{(0,k-1)}(s,t), \\ & H_{(k-1,0)}(s,t), H_{(k-1,k-1)}(s,t)] \end{aligned} \quad (6)$$

where the average [...] represents the averaging of the sub-blocks in the four corners being at the highest frequencies. These four sub-blocks are assumed to be occupied only by noise. Fig. 1 illustrates the described four corners in the case of $k=8$.

Finally, we perform the Wiener filtering operation. The Wiener filter, $W(s,t)$, is obtained by

$$W(s,t) = \frac{P_{(i,j)}(s,t)}{P_{(i,j)}(s,t) + N_{(i,j)}(s,t)}. \quad (7)$$

The power spectrum estimation method in this paper utilizes the image-wide Fourier transform instead of the localized Fourier transform. If this estimation employs the localized Fourier transform (by dividing the image into sub-blocks, and calculating the power spectrum of each sub-block (see Fig. 2(b)), the four corners in the sub-blocks do not always represent the highest frequencies of the whole image. For example, the sub-blocks containing the hat's feathers in Fig. 2(a) have a wide spread of energy at all frequencies. Therefore, if the four corners of these sub-blocks are considered as noise, this will lead to incorrect noise estimation. Conversely, the image-wide Fourier transform generates the power spectrum with the frequencies in the outmost image regions mostly occupied by noise. Therefore, the power spectrum of the outmost image regions are considered to be beneficial for the noise estimation.

In [24], the parameters k and λ are set to be 32 and 5, respectively. This is due to that when $\lambda=5$, it provides a robust and optimal restoration result for the FDWF in term of image fine details and edges preservation for different image characteristics and noise levels. When λ is fixed to 5, the threshold value α will be low. This setting will include higher frequencies in the estimated image power spectrum. It will contribute to the preservation of the image fine details and edges that usually occupy higher frequencies. Fig. 3 shows the close-up view of the restored Cameraman image and its logarithmic power spectrum (corrupted by the white noise with the variance, σ^2 , of 225) by using the FDWF with $\lambda=5$. From Fig. 3 we can observe that the FDWF has preserved the fine details and edges successfully, but has not effectively eliminated the noise in the restored image.

III. PROPOSED ALGORITHM

The method proposed in this paper reduces the noise in the image restored by using the FDWF with different parameters in the smooth and non-smooth regions. From our investigation, high threshold value setting in the FDWF reduces noise level. Conversely, low threshold value setting preserves the fine details and edges. We set out to improve the FDWF restoration performance by utilizing the advantage of both threshold settings. Fig. 4 shows a block diagram of our method. First, the noisy image is denoised with different weights of Wiener filtering to generate two restored images; one with highly reduced noise, and the other with preserved fine details and edges. Then, an edgemap image is generated directly from the noisy image. The two Wiener filtered images are utilized for the non-smooth and smooth regions based on the edgemap to generate the final restored image.

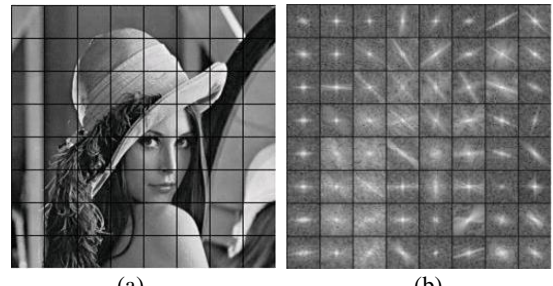


Fig. 2 (a) Lenna is divided into sub-blocks ($k=8$);
(b) localized Fourier transform for each sub-block of (a)

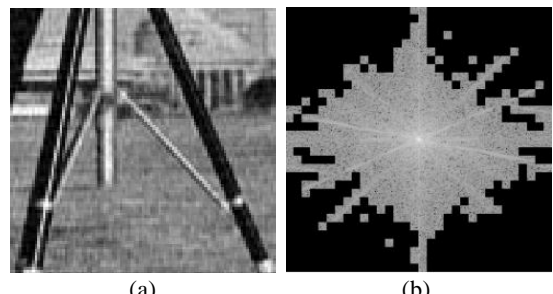


Fig. 3 Restored Cameraman and its logarithmic power spectrum ($\sigma^2=225$) by using FDWF ($\lambda=5$)

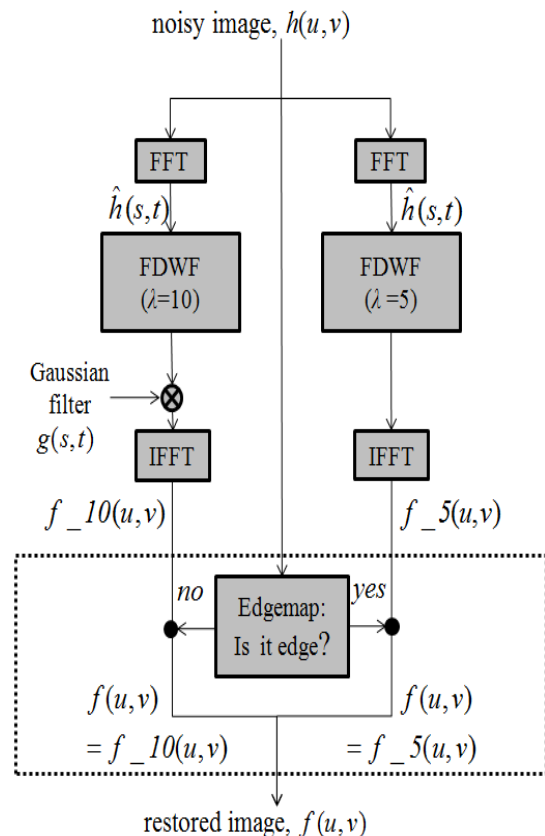


Fig. 4 Block diagram of proposed method

A. Image Restoration for Non-Smooth Regions

The image restored by the FDWF with $\lambda=5$ is inverse transformed to the spatial domain and represented as $f_5(u,v)$ hereafter. The $f_5(u,v)$ is utilized for the non-smooth regions in the final restored image, since it preserves the fine details and edges effectively.

B. Image Restoration for Smooth Regions

An image with highly reduced noise, which is restored by using the FDWF with high λ setting, is employed for the smooth regions in the final restored image. If λ is set to be high, the threshold value α will be high. This will allow the FDWF to threshold only the concentrated part of the low frequencies, which is assumed to be occupied only by the image power spectrum.

The most suitable λ setting that provides a restored image with considerably low noise level is selected by visual effects evaluation. From the preliminary investigation, we found that the FDWF with $\lambda=10$ provides the most suitable restored image. The restored image of Cameraman is shown in Fig. 5. From Fig. 5 we can observe that the noise level has been effectively reduced since noise is mostly cut out. On the other hand, the image is blurred since the edges in higher frequencies are cut out as well. Obvious ringing effects can be observed in the restored image, which is caused by sharp discontinuities at the threshold cutoff in the frequency domain. When the image is inverted into the spatial domain, it generates decreasing oscillations as it progresses outward from the center. The higher the threshold value, the stronger the oscillations will be.

To overcome the ringing effects, we multiply the output power spectrum filtered by the Wiener filter with a Gaussian lowpass filter. The restored image is inverse transformed to the spatial domain and denoted as $f_10(u,v)$. In Fig. 6, the ringing effects as seen in Fig. 5 are successfully suppressed. From our investigation, the best parameter settings for the Gaussian lowpass filter are fixed to the size of 128×128 with the standard deviation of 10.

C. Edgemap Construction

Next, the decomposition of the smooth and non-smooth regions is performed pixel-by-pixel based on an edgemap. This process has two advantages. First, the process is implemented without pre-processing, where the edgemap is constructed by executing edge detection directly from the noisy image in the spatial domain. Secondly, it requires minimum parameter setting, which is only the sub-block size for the image division. The process of the edgemap construction is as follows.

First, the noisy image is divided into $k \times k$ non-overlapping sub-blocks ($k=32$), each of which consists of 8×8 pixels. Next, the pixel value range, $r_{(i,j)}(u,v)$, of each sub-block (sub-blocks number = 32×32) is calculated as

$$r_{(i,j)}(u,v) = |(r_max - r_min)/2| \quad (8)$$

where r_max and r_min are the maximum and minimum values of the pixels in the corresponding sub-block, respectively. Then, the $r_{(i,j)}(u,v)$ that represents the minimum value of the entire $r_{(i,j)}(u,v)$, denoted as R , is determined by

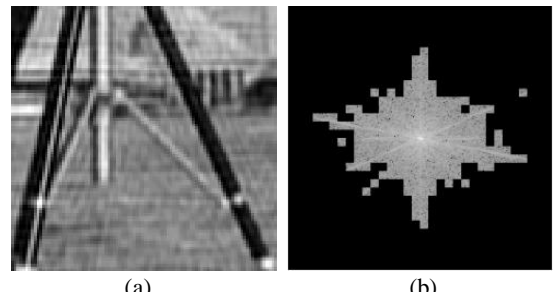


Fig. 5 Restored Cameraman and its logarithmic power spectrum ($\sigma^2=225$) by using FDWF ($\lambda=10$)

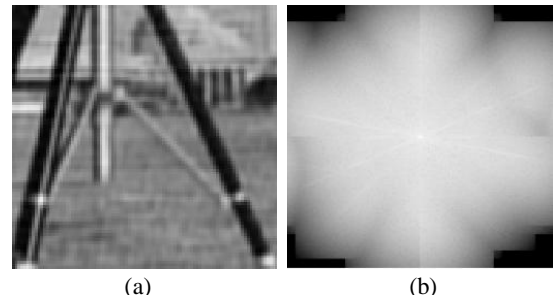
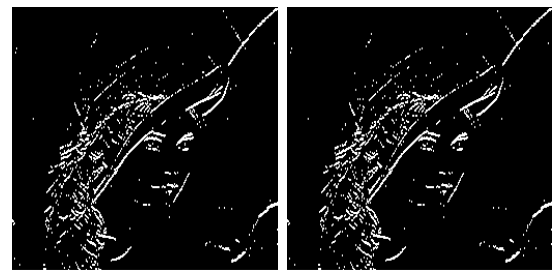
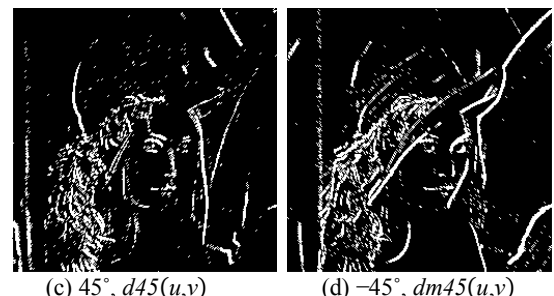


Fig. 6 Result for restored Cameraman ($\sigma^2=225$) by using FDWF ($\lambda=10$) multiplied with Gaussian lowpass filter



(a) horizontal, $dh(u,v)$ (b) vertical, $dv(u,v)$



(c) 45° , $d45(u,v)$ (d) -45° , $dm45(u,v)$



(e) $edgemap(u,v)$ (f) noisy Lenna
Fig. 7 Edgemap constructions in four directions and combined edgemap for noisy Lenna ($\sigma^2=225$)

$$R = \min(r_{(i,j)}(u,v)). \quad (9)$$

The sub-block with minimum $r_{(i,j)}(u,v)$ value is assumed to be homogeneous and represents the smooth region in the noisy image.

The edge detection is performed along a direction. Due to this, it will provide a more precise distinction between edges and noise in noisy environments because isolated pixels can be detected easier. The edge detection is performed in four directions. Four binary images are constructed from the edge detection in the horizontal, vertical, 45° , and -45° directions, which are defined as $dh(u,v)$, $dv(u,v)$, $d45(u,v)$, and $dm45(u,v)$, respectively. The binary images specifically are obtained as

$$dh(u,v) = \begin{cases} 1 & |h(u-1,v)-h(u,v)| > R \text{ or } |h(u,v)-h(u+1,v)| > R \\ 0 & \text{else} \end{cases} \quad (10)$$

$$dv(u,v) = \begin{cases} 1 & |h(u,v-1)-h(u,v)| > R \text{ or } |h(u,v)-h(u,v+1)| > R \\ 0 & \text{else} \end{cases} \quad (11)$$

$$d45(u,v) = \begin{cases} 1 & |h(u+1,v-1)-h(u,v)| > R \text{ or } |h(u,v)-h(u-1,v+1)| > R \\ 0 & \text{else} \end{cases} \quad (12)$$

$$dm45(u,v) = \begin{cases} 1 & |h(u-1,v-1)-h(u,v)| > R \text{ or } |h(u,v)-h(u+1,v+1)| > R \\ 0 & \text{else} \end{cases} \quad (13)$$

In order to determine whether a pixel in the noisy image belongs to a line along the edges, smooth region or additive noise, we consider the difference of corresponding pixel, $h(u,v)$ and its two neighbouring pixels in a direction. The distances are compared with R . For example, in horizontal direction as in (10), the difference between $h(u-1,v)$ and $h(u,v)$, and the difference between $h(u,v)$ and $h(u+1,v)$ are calculated. If any of the two differences is larger than R , the pixel $h(u,v)$ is considered as a part of a line along the edges. If both two differences are lower than R , the corresponding pixel $h(u,v)$ is assumed to belong to the smooth region or to be a pixel isolated from other non-smooth region's pixel (considered as noise).

As can be observed from Fig. 7 ((a)-(d)), the edges have been successfully detected from different directions, regardless of the high noise level (see Fig. 7(f)). However, the edge detection from only a single direction is not sufficient to represent all the edges for the entire image. Thus, we suggest to combine the edge detections of all four directions for obtaining a better result. The combined edgemap, $edgemap(u,v)$, is constructed by

$$edgemap(u,v) = \begin{cases} 1 & dh(u,v) \text{ or } dv(u,v) \text{ or } d45(u,v) \text{ or } dm45(u,v) > 0 \\ 0 & \text{else} \end{cases} \quad (14)$$

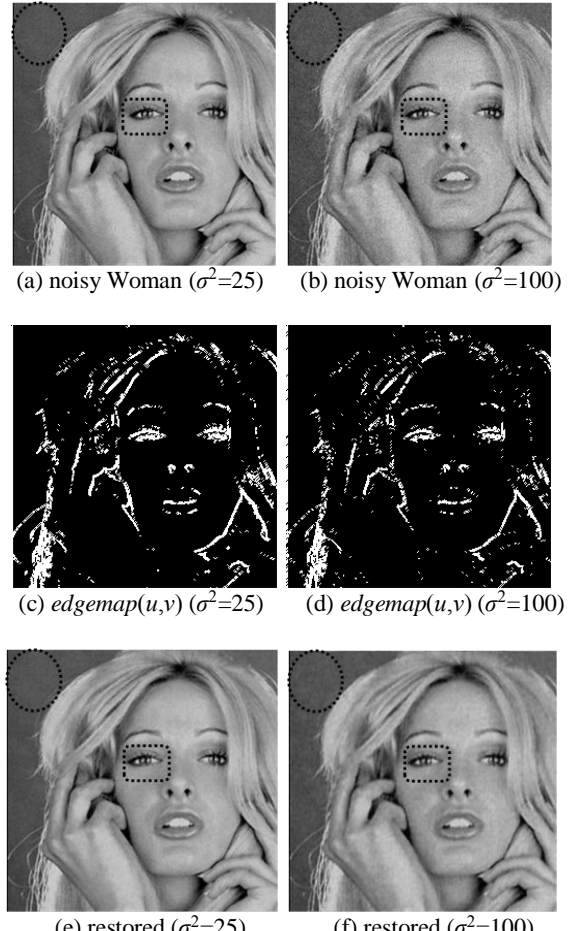


Fig. 8 Denoising for Woman image by using proposed method

Fig. 7(e) shows the edge detection of the $edgemap(u,v)$. Note that the $edgemap(u,v)$ provides relatively better edge detection along the lines in comparison with that of the single direction edge detection.

A. Edgemap-Based Image Restoration

The final restored image, $f(u,v)$, is constructed based on the edgemap as

$$f(u,v) = \begin{cases} f_{10}(u,v) & edgemap(u,v) = 0 \\ f_5(u,v) & edgemap(u,v) = 1 \end{cases} \quad (15)$$

If the $edgemap(u,v)$ is equal to 0, then the (u,v) th pixel of the final restored image $f(u,v)$ is assumed as the smooth region, and the (u,v) th pixel value of $f_{10}(u,v)$ is assigned to $f(u,v)$. Otherwise, the (u,v) th pixel value of $f_5(u,v)$ is assigned to $f(u,v)$. Fig. 8 shows the edgemap constructed directly from the noisy Woman image with $\sigma^2=25$ and 100, respectively. Note that by employing the edge detection approach in this paper, the edge detection has successfully distinguished most of the edges from noise in different noise levels. The edges are remained preserved while noise levels in smooth regions are better suppressed.

IV. RESULTS AND DISCUSSION

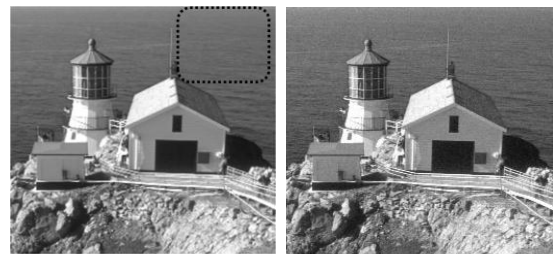
We have tested our method on nine grayscale test images (256×256) from the SIDBA database. All images are contami-

nated with additive Gaussian white noise ($\sigma^2=25$ and 100, and 225). The Airplane, Girl, Lenna, Woman and Boat images represent smooth natural images. The Barbara, Building, Lighthouse and Text images represent natural images that are highly rich in both fine details and edges. We investigate the performance of our method by using the mean measure of structural similarity (MSSIM) [25] since it is an image quality metric that well matches the human visual perception [25]. We also analyze the visual effects of the images. Each denoising method for comparison processes the test images with the same parameters setting (no tuning of parameters was performed for different noise level or image type).

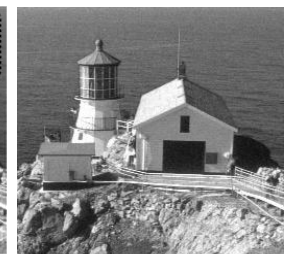
We have compared our method to two Wiener filters in different domains: the LBWDWF [16] and FDWF [24] in blind condition. In this paper, the LBWDWF with 4 vanishing moments (db4) lifting-based wavelet transform utilizes 3 decomposition levels and 3×3 filtering window. The FDWF employs the setting as in Section II. The objective evaluation results are tabulated in Tables I-III. Our method clearly outperforms the other two methods over the entire range of noise levels. Fig. 9(b)-(c) to Fig. 14(b)-(c) provide a visual comparison of tested images denoised using these two algorithms. Our method is capable to reduce more noise compared to the FDWF and provides better preservation of the original image features than that of the LBWDWF.

Finally, we have also compared our method to two state-of-the-art methods: the ATV [3] and NLM [4]. They are reported to have significant performance in preserving details while eliminating the noise. Both denoising methods are performed in ideal condition, where the noise variances are known. Conversely, our method estimates the noise employing the approach as in Section III. We perform the ATV based on the MATLAB code (default setting) as in [3]. In [4], the NLM suggested using the search window size of 21×21 and similarity window of 7×7 for images with the size of 512×512 . However, the parameters setting as in [4] results in over-smoothed restored images for small resolution test image (256×256). Thus, we set the search window and similarity window for the NLM to 5×5 and 2×2 , respectively for obtaining better denoising results. From Tables I-III, note that our method is better than the ATV in most of the cases. Our method is also better than the NLM in many images that are highly rich in both fine details and edges. Fig. 9(e)-(f) to Fig. 14(e)-(f) provide a visual comparison of tested images denoised using these two algorithms. In higher noise level, as can be seen in Fig. 11(e)-(f) and Fig. 14(e)-(f), the ATV and NLM result in strong noise removal. However, they eliminate the fine details and edges at the same time. Our method reduces a considerable amount of noise and furthermore preserves fine details and edges better than the NLM and ATV. The investigation validates that our method with the proposed noise estimation technique provides a comparable performance with the state-of-the-arts methods performed in ideal condition.

Table IV shows the execution time for each denoising method implemented in MATLAB computed on a 1.4 GHz Intel Core 2 Duo CPU. The execution time of our method is slightly higher than that of the LBWDWF, but considerably lower when compared to that of the ATV and NLM.



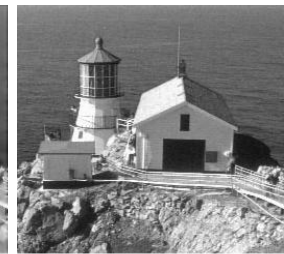
(a) Original



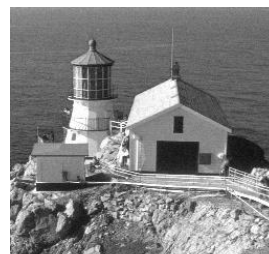
(b) FDWF



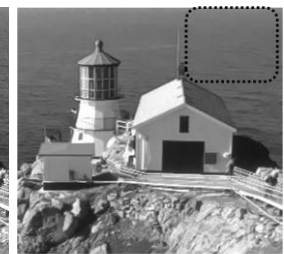
(c) LBWDWF



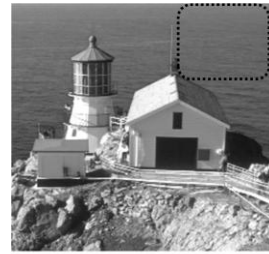
(d) Proposed



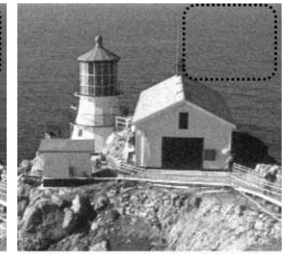
(e) ATV



(f) NLM

Fig. 9 Restoration comparison of Lighthouse with low noise level ($\sigma^2=25$)

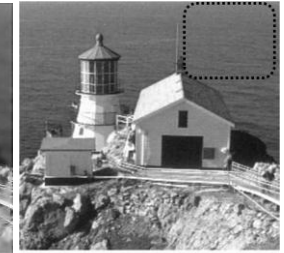
(a) Original



(b) FDWF



(c) LBWDWF



(d) Proposed

V. CONCLUSION

We have proposed a denoising approach in blind condition that is effective for preserving the image fine details and edges while reducing the noise levels in the restored images. From the study, it is found that our method is fast and more suitable for denoising images that are rich in both fine details and edges.

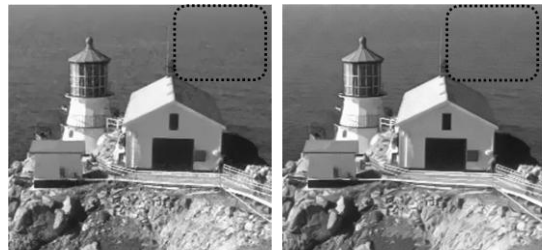
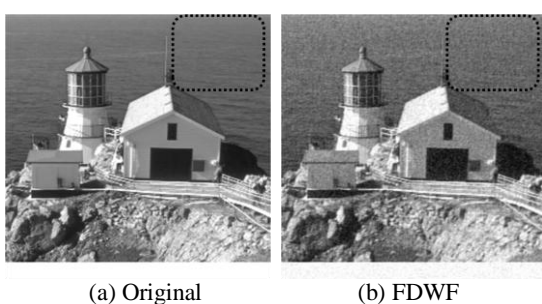
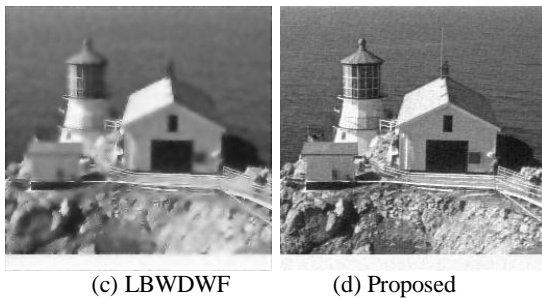


Fig. 10 Restoration comparison of Lighthouse with moderate noise level ($\sigma^2=100$)



(a) Original (b) FDWF



(c) LBWDWF (d) Proposed

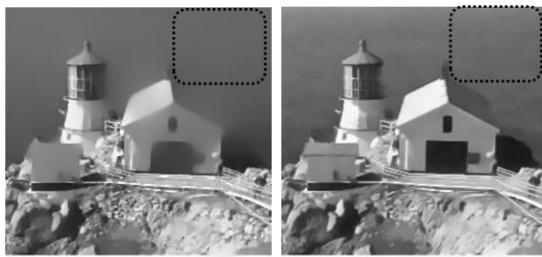
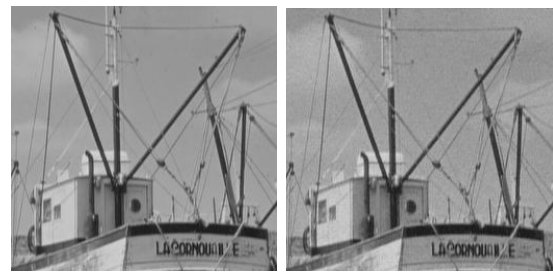
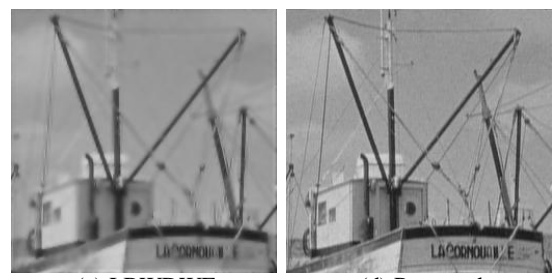


Fig. 11 Restoration comparison of Lighthouse with high noise level ($\sigma^2=225$)



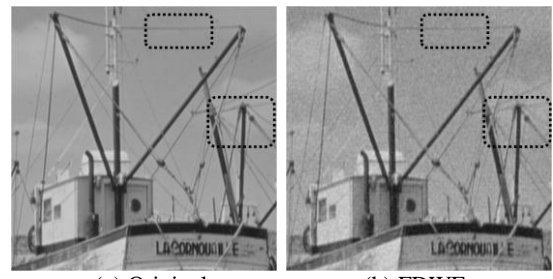
(a) Original (b) FDWF



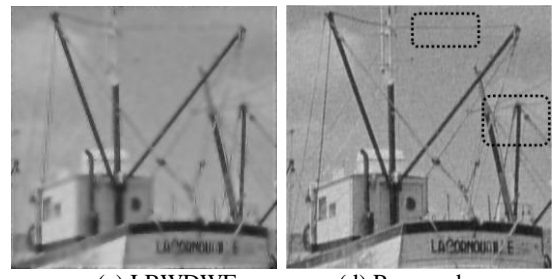
(c) LBWDWF (d) Proposed



(e) ATV (f) NLM
Fig. 12 Restoration comparison of Boat with low noise level ($\sigma^2=25$)



(a) Original (b) FDWF



(c) LBWDWF (d) Proposed

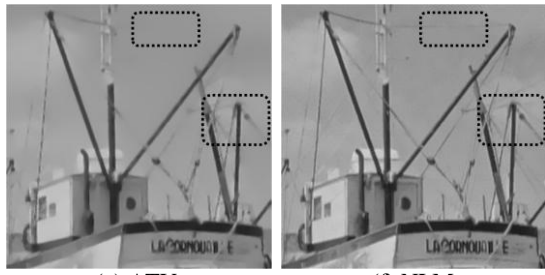


Fig. 13. Restoration comparison of Boat with moderate noise level ($\sigma^2=100$)

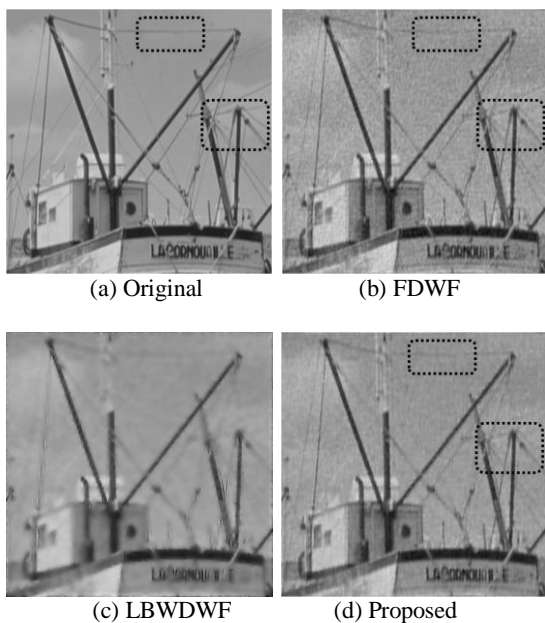


Fig. 14. Restoration comparison of Boat with high noise level ($\sigma^2=225$)

REFERENCES

- [1] C. H. Hsieh, P. C. Huang and S. Y. Hung, "Noisy image restoration based on boundary resetting BDND and median filtering with smallest window," *WSEAS Trans. Signal Processing*, vol.5, no.5, pp. 178–187, May 2009.
- [2] V. Gui and C. Caleanu, "On the effectiveness of multiscale mode filters in edge preserving," in *Proc. WSEAS Int. Conf. Systems*, Rodos Island, 2009, pp. 190–195.
- [3] G. Gilboa, N. Sochen, and Y. Zeevi, "Texture preserving variational denoising using an adaptive fidelity term," in *Proc. IEEE Workshop Variational and Level Set Methods in Computer Vision*, Nice, 2003, pp.137–144. Available:http://visl.technion.ac.il/~gilboa/PDE-filt/demo.adap_tv.m.
- [4] A. Buades, B. Coll, and J.M. Morel, "A non-local algorithm for image denoising," in *Proc. IEEE Int. Conf. Computer Vision and Pattern*

Table I Performance comparison in MSSIM ($\sigma^2=25$)

Test images	LBW DWF (blind)	FD WF (blind)	Propo -sed (blind)	ATV (ideal)	NLM (ideal)
Barbara	0.67	0.95	0.96	0.94	0.97
Building	0.62	0.96	0.96	0.96	0.96
Lighthouse	0.68	0.91	0.94	0.90	0.93
Text	0.68	0.95	0.96	0.95	0.93
Airplane	0.81	0.89	0.92	0.95	0.94
Girl	0.82	0.91	0.92	0.91	0.93
Lenna	0.83	0.91	0.94	0.96	0.96
Woman	0.81	0.91	0.94	0.95	0.95
Boat	0.79	0.93	0.94	0.93	0.96

Table II Performance comparison in MSSIM ($\sigma^2=100$)

Test images	LBW DWF (blind)	FD WF (blind)	Propo -sed (blind)	ATV (ideal)	NLM (ideal)
Barbara	0.66	0.88	0.90	0.90	0.93
Building	0.62	0.89	0.91	0.90	0.91
Lighthouse	0.67	0.80	0.86	0.90	0.89
Text	0.68	0.88	0.89	0.90	0.88
Airplane	0.80	0.77	0.85	0.92	0.91
Girl	0.81	0.83	0.87	0.81	0.89
Lenna	0.82	0.82	0.88	0.92	0.92
Woman	0.80	0.82	0.87	0.90	0.91
Boat	0.78	0.84	0.88	0.86	0.92

Table III Performance comparison in MSSIM ($\sigma^2=225$)

Test images	LBW DWF (blind)	FD WF (blind)	Propo -sed (blind)	ATV (ideal)	NLM (ideal)
Barbara	0.66	0.82	0.85	0.41	0.84
Building	0.61	0.84	0.84	0.56	0.76
Lighthouse	0.66	0.72	0.79	0.75	0.79
Text	0.67	0.82	0.84	0.72	0.80
Airplane	0.78	0.70	0.78	0.58	0.86
Girl	0.80	0.77	0.81	0.55	0.82
Lenna	0.81	0.75	0.84	0.5	0.86
Woman	0.79	0.75	0.83	0.47	0.84
Boat	0.76	0.77	0.82	0.52	0.84

Table IV Average time execution (s)

Noise, σ^2	LBW DWF (blind)	FD WF (blind)	Propo -sed (blind)	ATV (ideal)	NLM (ideal)
25	0.60	0.31	0.93	23.33	67.31
100	0.56	0.31	0.92	66.17	68.60
225	0.57	0.30	0.93	751.49	67.82

- Recognition*, San Diego, 2005, vol.2, pp. 60–65.
- [5] R. Gomathi and S. Selvakumaran, “A bivariate shrinkage function for complex dual tree DWT based image denoising,” in *Proc. WSEAS Int. Conf. Wavelet Analysis & Multirate Systems*, Bucharest, 2006, pp. 36–40.
- [6] N. Wiener, *Extrapolation, Interpolation, and Smoothing of Stationary Time Series*. Cambridge: Wiley, 1949, ch. 3.
- [7] R. C. Gonzalez, R. E. Woods and S. L. Eddins, *Digital Image Processing using MATLAB*. New Jersey: Prentice Hall, 2004, ch. 5.
- [8] J. S. Lee, “Digital image enhancement and noise filtering by use of local statistics,” *IEEE Trans. Pattern Analysis and Machine Intelligent*, vol.PAMI-2, no.2, pp. 165–168, Mar. 1980.
- [9] A. D. Hillery, and R. T. Chin, “Iterative Wiener filters for image restoration,” *IEEE Trans. Signal Processing*, vol.39, no.8, pp. 1892–1899, Aug. 1991.
- [10] H. Furuya, S. Eda and T. Shimamura, “Image restoration via Wiener filtering in the frequency domain,” *WSEAS Trans. Signal Processing*, vol.5, no.2, pp. 63–73, Feb. 2009.
- [11] J. S. Lim, *Two-Dimensional Signal and Image Processing*. New Jersey: Prentice Hall, 1990, ch. 6.
- [12] V. Bruni, and D. Vitulano, “A Wiener filter improvement combining wavelet domains,” in *Proc. IEEE Int. Conf. Image Analysis and Processing*, Montavolo, 2003, pp. 518–523.
- [13] P. L. Shui, “Image denoising algorithm via doubly local Wiener filtering with directional windows in wavelet domain,” *IEEE Signal Processing Letter*, vol.12, no.10, pp. 681–684, Oct. 2005.
- [14] W. Sweldens, “The lifting scheme: a construction of second-generation wavelets,” *SIAM Journal Mathematics Analysis*, vol.29, no.2, pp. 511–546, May 1997.
- [15] I. Daubechies, and W. Sweldens, “Factoring wavelet transforms into lifting steps,” *Journal Fourier Analysis Application*, vol.4, no.3, pp. 247–269, May 1998.
- [16] E. Ercelebi and S. Koc, “Lifting-based wavelet domain adaptive Wiener filter for image enhancement,” *IEE Proc. Vis. Image and Signal Processing*, vol.153, no.1, pp. 31–36, Feb. 2006.
- [17] F. Jin, P. Fieguth, L. Winger and E. Jernigan, “Adaptive Wiener filtering of noisy images and image sequences,” in *Proc. IEEE Int. Conf. Image Processing*, Barcelona, 2003, pp. 349–52.
- [18] Z. Lu, G. Hu, X. Wang and L. Yang, “An improved adaptive Wiener filtering algorithm,” in *Proc. IEEE Int. Conf. Signal Processing*, Beijing, 2006, pp. 60–65.
- [19] J. S. Lim and N. A. Malik, “A new algorithm for two-dimensional maximum entropy power spectrum estimation,” *IEEE Trans. Acoustic Speech, and Signal Processing*, vol.29, no.3, pp. 401–413, June 1981.
- [20] J. S. Lim and F.U. Dowla, “A new algorithm for high-resolution two-dimensional spectral estimation,” *Proc. IEEE*, vol.71, no.2, pp. 284–285, Feb. 1983.
- [21] T. Kobayashi, T. Shimamura, T. Hosoya and Y. Takahashi, “Restoration from image degraded by white noise based on iterative spectral subtraction method,” in *Proc. IEEE Int. Symposium Circuits and Systems*, Kobe, 2005, pp. 6268–6271.
- [22] P. Sysel, and J. Misurec, “Estimation of power spectral density using wavelet thresholding,” in *Proc. WSEAS Int. Conf. Circuits, Systems, Electronics, Control and Signal Processing*, Canary Island, 2008, pp. 207–211.
- [23] L. Rudin, S. Osher and E. Fatemi, “Nonlinear total variation based noise removal algorithms,” *Physica D*, vol.60, pp. 259–268, Nov. 1992.
- [24] S. Suhaila and T. Shimamura, “Power spectrum estimation method for image denoising by frequency domain Wiener filter,” in *Proc. IEEE Int. Conf. Computer and Automation Engineering*, Singapore, 2010, pp. 608–612.
- [25] Z. Wang, A. C. Bovik, H.R. Sheikh and E. P. Simoncelli, “Image quality assessment: from error visibility to structural similarity,” *IEEE Trans. Image Processing*, vol.13, no.4, pp. 600–612, Apr. 2004.